

Supporting Information

# Terahertz scanning tunneling microscopy for visualizing ultrafast electron motion in nanoscale potential variations

*Shoji. Yoshida<sup>1</sup>, Yusuke. Arashida<sup>1</sup>, Hideki Hirori<sup>2</sup>, Takehiro. Tachizaki<sup>3</sup>, Atsushi.*

*Taninaka<sup>1</sup>, Hiroki Ueno<sup>1</sup>, Osamu Takeuchi<sup>1</sup>, and Hidemi Shigekawa<sup>1\*</sup>*

<sup>1</sup>Faculty of Pure and Applied Sciences, University of Tsukuba, Tsukuba 305-8573, Japan

<sup>2</sup>Institute for Chemical Research, Kyoto University, Uji, Kyoto, 611-0011

<sup>3</sup>Department of Optical and Imaging Science and Technology, Tokai University, Hiratsuka-shi,  
Kanagawa, 259-1292, Japan

\*Correspondence should be addressed to H.S. (hidemi@ims.tsukuba.ac.jp).

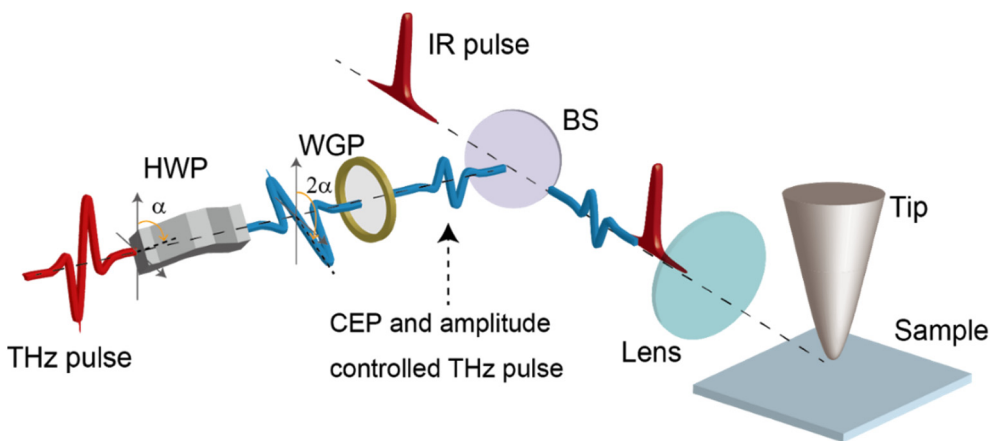


**Fig. S1. Schematic illustration of electric field strength control system.** A LiNbO<sub>3</sub> crystal was excited using an optical pulses output (1035 nm, 40 W, 309 fs, 50 MHz repetition rate) from a femtosecond laser (Coherent Monaco) with the tilted pulse front technique to generate and THz pulses (1). We used THz CEP shifter (Hamamatsu photonics) as a half waveplate (HWP) to rotate the polarization angle of THz pulse (2). The polarization angle of the THz pulse changes by  $2\alpha$  depending on the rotation angle  $\alpha$  of the HWP. Therefore, when  $\alpha$  is changed from  $0^\circ$  to  $\pi/2$ , the polarization angle of the THz pulse changes from  $0^\circ$  to  $\pi$ . After that, a wire grid polarizer (WGP) is used to transmit only the polarized component along the STM probe axis (S polarized light). The CEP of the THz pulse after WGP can be set to two values, 0 or  $\pi$ . After that, the THz pulse was merged coaxially with the infrared pulse for sample excitation using the THz/Vis beam splitter (BS), and the THz lens installed in the ultra-high vacuum STM chamber (Tsurupica,  $f = 100$  mm) is used to illuminate the STM tunnel junction.

A simple estimate of the number of photons and excited electrons was made. We estimated the number of photon and excited electrons. With a laser power of 10 mW and a repetition frequency of 16.6 MHz, the number of photons per pulse is about  $3 \times 10^9$ . Assuming the spot size of 10  $\mu\text{m}$  diameter, the number of photons in the rage of 10 nm diameter is 3000. The reflectance (1035 nm) of the Au surface is 96.5%, and if all the loss is used for electronic excitation, one electron is excited per 1 nm x 1 nm. It is not clear how many electrons will be injected into LUMO, but if the measured THz current is 1 pA, the number of electrons per pulse becomes 0.4, which is almost of the same order with the experimental value. The effects of tip enhancement and the lateral diffusion are not considered here.

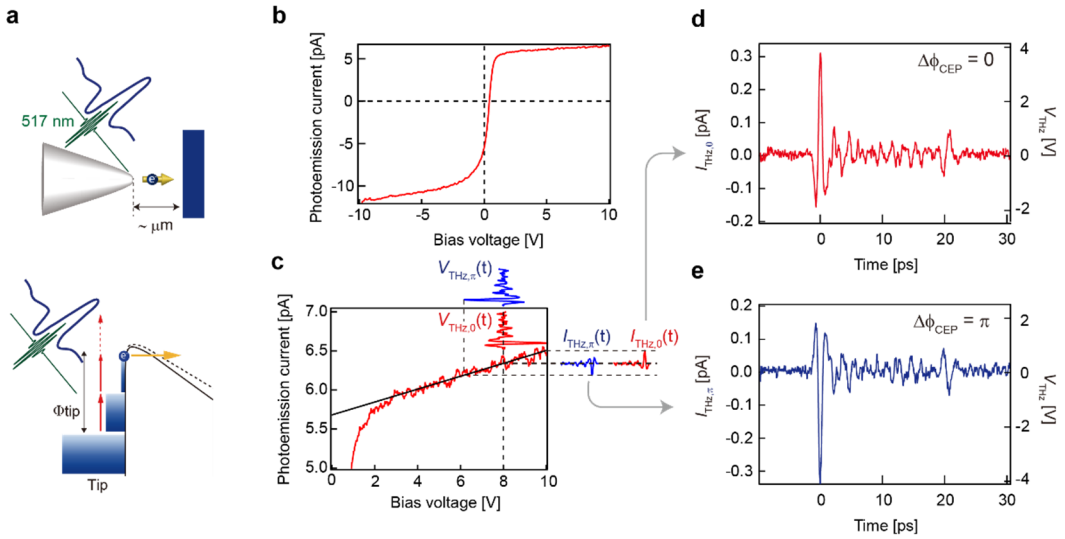


**Fig. S2. Method for measuring THz near-field waveform using photoemission.** (a) Schematics of the measurement setup and the band diagram near the STM tip. (b) Typical  $I$ - $V$  curve obtained by photoelectron current. (c) Magnified view of (b) for the positive side. The black line shows the fitting of the linear region.  $I_{\text{THz},0}$  and  $I_{\text{THz},\pi}$  are the THz currents induced by the THz electric field for  $\Phi = 0$  and  $\pi$ , respectively. (d) and (e) Magnifications of  $I_{\text{THz},0}$  and  $I_{\text{THz},\pi}$  shown in (c), respectively.

As shown in Fig. S2a, when the STM probe and sample are irradiated by a strong visible (517 nm 10 mJ/cm<sup>2</sup>, 1 MHz) pulse produced by the second harmonic generation (SHG) of fundamental pulse, some of the hot electrons excited by multiphoton absorption overcome the barrier and photoemission from both surfaces occurs. The  $I$ - $V$  curve measured with the tip-sample distance of 1 μm is shown in Fig. S2b. The photoelectron current changes with the applied bias voltage, and photoelectrons generated on the tip surface flow into the sample at a high positive voltage. As shown in Fig. S2c, a magnification of b, the  $I$ - $V$  curve is almost linear above  $V_{\text{DC}} = 4$  V. Therefore, when  $V_{\text{DC}}$  is set to +8 V, within this linear region, and the THz pulse is applied during the excitation by the IR pulse, the photoelectron current changes linearly with the magnitude of the THz electric field. Since the lifetime of hot electrons is very short ( $\sim 100$  fs),  $I_{\text{THz}}$  is proportional to the THz electric field during the IR excitation.  $I_{\text{THz}}(t_d)$  is shown for  $\Delta\Phi = 0$  and  $\pi$  in Figs. S2d and S2e, respectively. The shape of  $I_{\text{THz}}(t_d)$  is similar to the THz near-field waveform at the tip, i.e.,  $I_{\text{THz}} = \alpha V_{\text{THz}}$ . The proportional coefficient  $\alpha$  is obtained from the slope of the linear region in Fig. S2c. Thus, it is possible to convert  $I_{\text{THz}}$  to  $V_{\text{THz}}$  using this relationship (3,4).

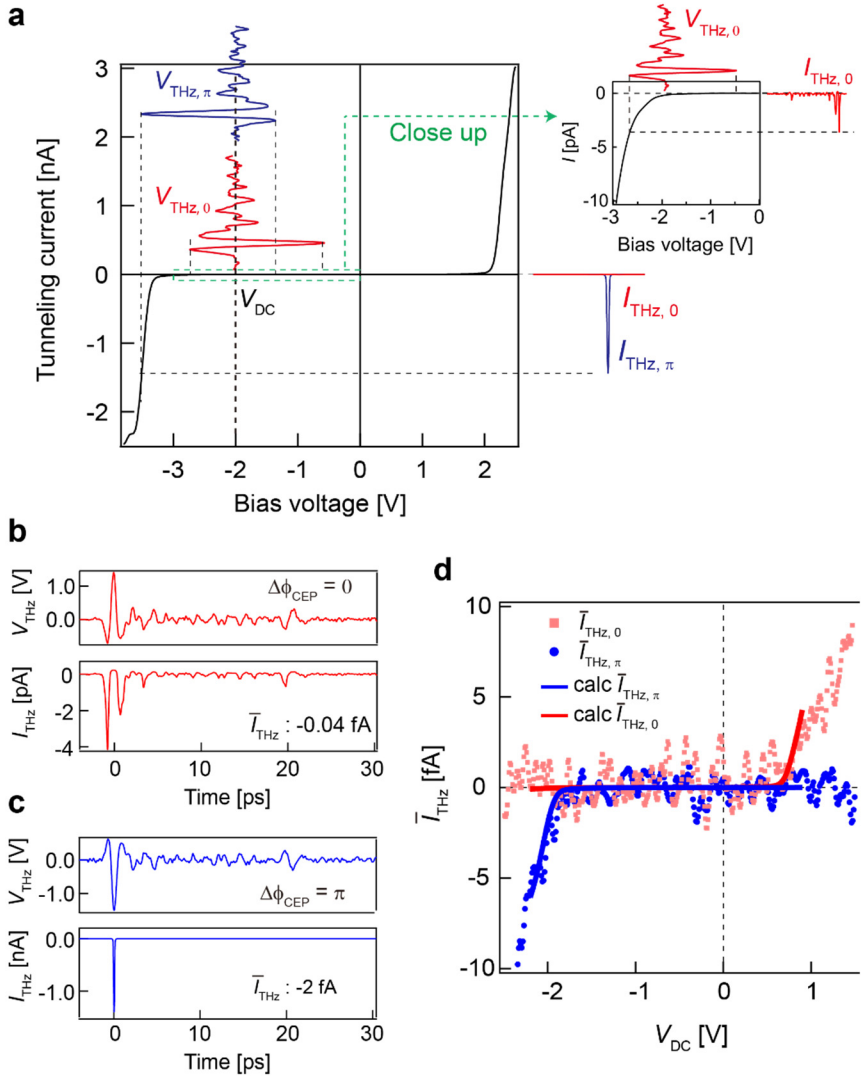


**Fig. S3. Derivation of THz voltage in tunnel region.** (a) Typical static  $I$ - $V$  curve measured over a wide voltage range (setpoint:  $V_S = -3.0$  V,  $I_t = 10$  pA). The relationship between the voltage  $V_{\text{THz}}$  produced by the THz electric field and the THz-induced current  $I_{\text{THz}}$  is also shown. (b), (c) Waveforms of  $V_{\text{THz}}$  and  $I_{\text{THz}}$  calculated using  $V_{\text{THz}}$  for ( $\Delta\Phi = \pi$ ,  $V_{\text{DC}} = -2.0$  V,  $V_{\text{THz-peak}} = 1.5$  V) and ( $\Delta\Phi = \pi$ ,  $V_{\text{DC}} = -2.0$  V,  $V_{\text{THz-peak}} = -1.5$  V), respectively. (d) Calculated (solid line) and measured (dots)  $I_{\text{THz}}$ - $V_{\text{DC}}$  curves.  $I_{\text{THz},0}$  and  $I_{\text{THz},\pi}$  are THz currents for  $\Delta\Phi = 0$  and  $\pi$ , respectively.

To understand the origin of  $I_{\text{THz}}$  in the time-resolved THz-STM experiment, we need to know the magnitude of  $V_{\text{THz}}$  applied between the STM tip and sample in a tunneling regime. Therefore, we carried out  $I_{\text{THz}}$ - $V_{\text{DC}}$  measurement to calibrate the magnitude of  $V_{\text{THz}}$ . Figures S3a and S3b show the basic concept of the analysis. The experimental  $I_{\text{THz}}$  is time-averaged as shown by the following equation:

$$I_{\text{THz}}(V_{\text{DC}}, t_d) = f_{\text{rep}} \int_{t_d}^{t_d + 1/f_{\text{rep}}} [I\{V_{\text{DC}} + V_{\text{THz}}(t)\} - I(V_{\text{DC}})] dt, \quad (1)$$

Therefore, in principle, we can calculate  $I_{\text{THz}}$  at a particular voltage  $V_{\text{DC}}$  based on the static

*I*-*V* curve and  $V_{\text{THz}}(t)$ . To obtain the magnitude of  $V_{\text{THz}}$ , we first measured  $I_{\text{THz}}$ - $V_{\text{DC}}$  curves using  $V_{\text{THz}}$  for two CEPs ( $V_{\text{THz},0}$  and  $V_{\text{THz},\pi}$ ), then we performed curve fitting using the numerically calculated  $I_{\text{THz}}$ - $V_{\text{DC}}$  curve with the magnitude of  $V_{\text{THz}}$  as an independent variable. Best fitting was obtained when the peak of  $V_{\text{THz}}$  ( $V_{\text{THz-peak}}$ ) is equal to  $\pm 1.5$  V. as shown in Fig. S3d, The positions of the rising voltage of  $I_{\text{THz}}$  and the magnitude of  $I_{\text{THz}}$  show good agreement with each other.

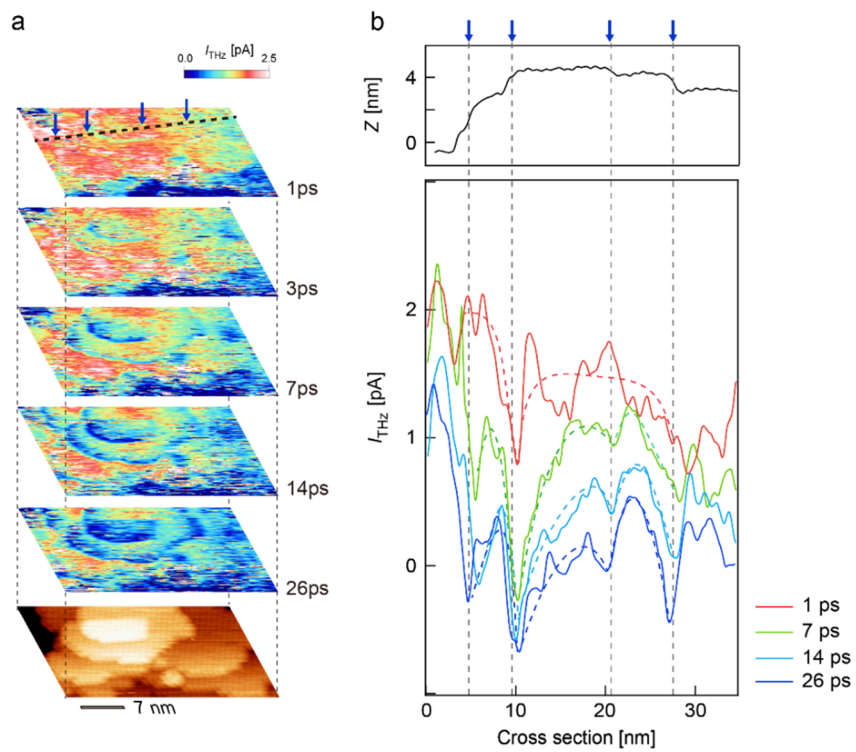


**Fig. S4.** (a) Time-resolved images of electron motion obtained over a large area, showing the generality of the observed phenomena. (b) Delay time dependence of the profile along the dotted line in (a). The gradual decreases in the high-density area can be seen, showing the existence of the horizontal diffusion process faster than the vertical diffusion. Blue arrows indicate the positions of the step edges crossing the dotted line.

**Movie S1.** Movie showing the motion of electrons obtained in the same area of fig.S4.

## REFERENCES

- (1) Hirori, H.; Doi, A.; Blanchard, F.; Tanaka, K. Single-Cycle Terahertz Pulses with Amplitudes Exceeding 1 MV/cm Generated by Optical Rectification in LiNbO<sub>3</sub>. *Appl. Phys. Lett.* **2011**, *98*, 091106.
- (2) Kawata, Y.; Yasuda, T.; Takahashi, H. Carrier Envelope Phase Shifter for Broadband Terahertz Pulses. *Opt. Lett.* **2016**, *41*, 986–989.
- (3) Yoshida, S.; Hirori, H.; Tachizaki, T.; Yoshioka, K.; Arashida, Y.; Wang, Z. H.; Sanari, Y.; Takeuchi, O.; Kanemitsu, Y.; Shigekawa, H. Subcycle Transient Scanning Tunneling Spectroscopy with Visualization of Enhanced Terahertz Near Field. *ACS Photonics* **2019**, *6*, 1356–1364.
- (4) Müller, M.; Martín-Sabanés, N.; Kampfrath, T.; Wolf, M. Phase-Resolved Detection and Control of Ultrabroadband THz Pulses Coupled to a Scanning Tunneling Microscope Junction. *ACS Photonics* **2020**, *7*, 2046–2055.